nature biotechnology

Single base–resolution methylome of the silkworm reveals a sparse epigenomic map

Hui Xiang[1,2,10], Jingde Zhu[3,4,10], Quan Chen[2,10], Fangyin Dai[5,10], Xin Li[1,10], Muwang Li[6], Hongyu Zhang[3], Guojie Zhang[2], Dong Li[5], Yang Dong[1], Li Zhao[1], Ying Lin[5], Daojun Cheng[5], Jian Yu[3], Jinfeng Sun[3], Xiaoyu Zhou[3], Kelong Ma[3], Yinghua He[3], Yangxing Zhao[3], Shicheng Guo[3], Mingzhi Ye[2], Guangwu Guo[2], Yingrui Li[2], Ruiqiang Li[2], Xiuqing Zhang[2], Lijia Ma[2], Karsten Kristiansen[7], Qiuhong Guo[8], Jianhao Jiang[8], Stephan Beck[9], Qingyou Xia[5], Wen Wang[1] & Jun Wang[2,7]

Epigenetic regulation in insects may have effects on diverse biological processes. Here we survey the methylome of a model insect, the silkworm *Bombyx mori*, at single-base resolution using Illumina high-throughput bisulfite sequencing (MethylC-Seq). We conservatively estimate that 0.11% of genomic cytosines are methylcytosines, all of which probably occur in CG dinucleotides. CG methylation is substantially enriched in gene bodies and is positively correlated with gene expression levels, suggesting it has a positive role in gene transcription. We find that transposable elements, promoters and ribosomal DNAs are hypomethylated, but in contrast, genomic loci matching small RNAs in gene bodies are densely methylated. This work contributes to our understanding of epigenetics in insects, and in contrast to previous studies of the highly methylated genomes of *Arabidopsis*[1] and human[2], demonstrates a strategy for sequencing the epigenomes of organisms such as insects that have low levels of methylation.

The recently developed MethylC-Seq[1] technology couples bisulfite-based detection of methylated cytosines to high-throughput whole-genome sequencing. Application of this technology to *Arabidopsis*[1] and humans[2] has revealed that these species are highly methylated (about 5% genomic cytosines), and the high resolution of these studies identified new elaborate patterns and functional effects of DNA methylation.

Insects, however, seem to have lower levels of methylation[3], with ~0.15–0.19% of DNA being methylated in the silk gland of the silkworm (*Bombyx mori*)[4], as assayed by high-performance liquid chromatography, and even lower levels observed in flies, mosquitoes and honeybees[3,4]. The feasibility of performing MethylC-Seq on organisms with such low methylation levels has not yet been evaluated. Recent interest in DNA methylation in insects has been sparked by evidence for the existence both of active methyltransferase enzymes, which attach methyl groups to DNA, and of methylated genes in *Drosophila*, the aphid *Myzus persicae* and particularly the honeybee *Apis mellifica*[5–7]. The absence of comprehensive genome-wide profiling and functional analysis of DNA methylation in insects, however, has hindered our understanding of epigenetic regulation in these organisms.

The silkworm, which has been subjected to domestication for 5,000 years[8], is an economically important model insect of Lepidoptera, an order that includes many crop pests, such as the cotton bollworm. As an alternative mechanism to mutations in germline DNA, epigenetic changes via DNA methylation called epimutations have been reported to influence ecologically favorable traits, and thus species evolution, in both plants and mammals[9,10]. Therefore, the silkworm could be a valuable model, not only for studying functional effects of DNA methylation in insects but also for exploring the effects of epigenetics during domestication.

The number of DNA methyltransferase enzymes encoded in the genomes of different insect species varies greatly[11]. In the silkworm (*B. mori*), previous studies[11,12] identified two DNA methyltransferase genes (*dnmt1* and *dnmt2*) and experimentally characterized the methyl DNA–binding protein MBD2/3, providing intriguing evidence for the presence of DNA methylation in this insect species. We conducted extensive searches in the silkworm genome and confirmed that there are only *dnmt1* and *dnmt2* DNA methyltransferase genes (*Bmdnmt1* and *Bmdnmt2*). Our PCR experiments with reverse transcription (RT-PCR) show that the two silkworm methyltransferase genes are expressed in a development- and tissue-regulated pattern (**Supplementary Fig. 1a**). Nuclear protein extracts from early embryos (8-h eggs) and silk glands further demonstrate the presence of catalytic activity of DNA methylation in silkworms (**Supplementary Fig. 1b**).
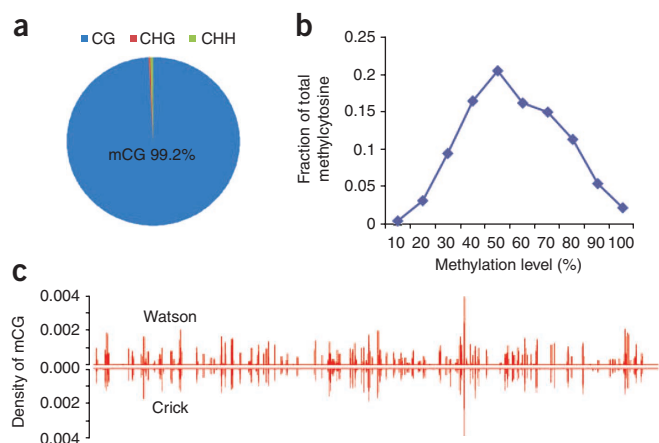
Figure 1 DNA methylation patterns and chromosomal distribution in *Bombyx mori*. (**a**) Fraction of mCs identified in each sequence context for the strain *Dazao*, indicating rather low and non-CG methylation, which are likely to be false positives. (**b**) Distribution of mCs (*y* axis) across methylation levels (*x* axis). Methylation level was determined by dividing the number of reads covering each mC by the total reads covering that cytosine. (**c**) Density of mCs identified on the two DNA strands (Watson and Crick) throughout chromosome 1 (out of 28). Density was calculated in 25-kb bins. The value refers to the number of mCs per base pair, as shown on the *y* axis.

The above results led us to apply MethylC-Seq to reveal the genome-wide DNA methylation pattern in the silkworm. First, we sequenced bisulfite-treated total DNA, extracted from the silk gland of an individual of the *Dazao* strain, whose genome has already been sequenced[13]. In total, 272,312,422 raw reads were produced (**Supplementary Table 1**). After removing low-quality and clonal reads, we obtained 133,765,113 effective reads, and the sequence yield for final analysis was 5.9 gigabase pairs (Gb), covering 92% of all cytosines in the genome with an average depth 7.4 × per strand (**Supplementary Table 1**). Initially we observed overall genome-wide methylation levels of 0.67% at CG, 0.21% at CHG and 0.24% at CHH sites (H = A, C or T), indicating higher CG methylation than non-CG methylation.

Because non-CG methylation is reported to be either very rare or nonexistent in honeybees[6], we selected a series of genomic regions to validate our initial results. Based on the MethylC-Seq results, we picked five genomic regions that contain 26 mCGs, as well as three regions that contain 98 clustered mCHHs and one mCHG. In these regions, we performed traditional bisulfite-PCR and sequencing validation (BS-PCR). Notably, although 92.3% of the methylated cytosines (mCs) at CG sites were validated, none of the non-CG mCs were validated by the BS-PCR (**Supplementary Table 2**).

To further confirm this result, we validated a larger batch of regions with methylation sites (692 CGs, 29 CHGs and 63 CHHs, respectively) using BS-PCR followed by 454 sequencing (454 Life Sciences). Similarly, a high percentage of CG methylations were validated (82.9%) but none of the non-CG mCs (**Supplementary Table 2**). These results suggest that non-CG mCs are either nonexistent or very rare in the silkworm, as was found in the honeybee[6]. To account for this fact, we used the non-CG mC rate as the background control[2] to calculate the false-positive rate (non-conversion and thymidine-to-cytosine sequencing errors), the value of which is estimated to be 0.23%. After corrections based on this value, we identified 600,422 mCs, accounting for 0.40% of all genomic cytosines. Unfortunately,

about 45% of these mCs were at non-CG sites, indicating that false mCs were still prevalent even after this correction.
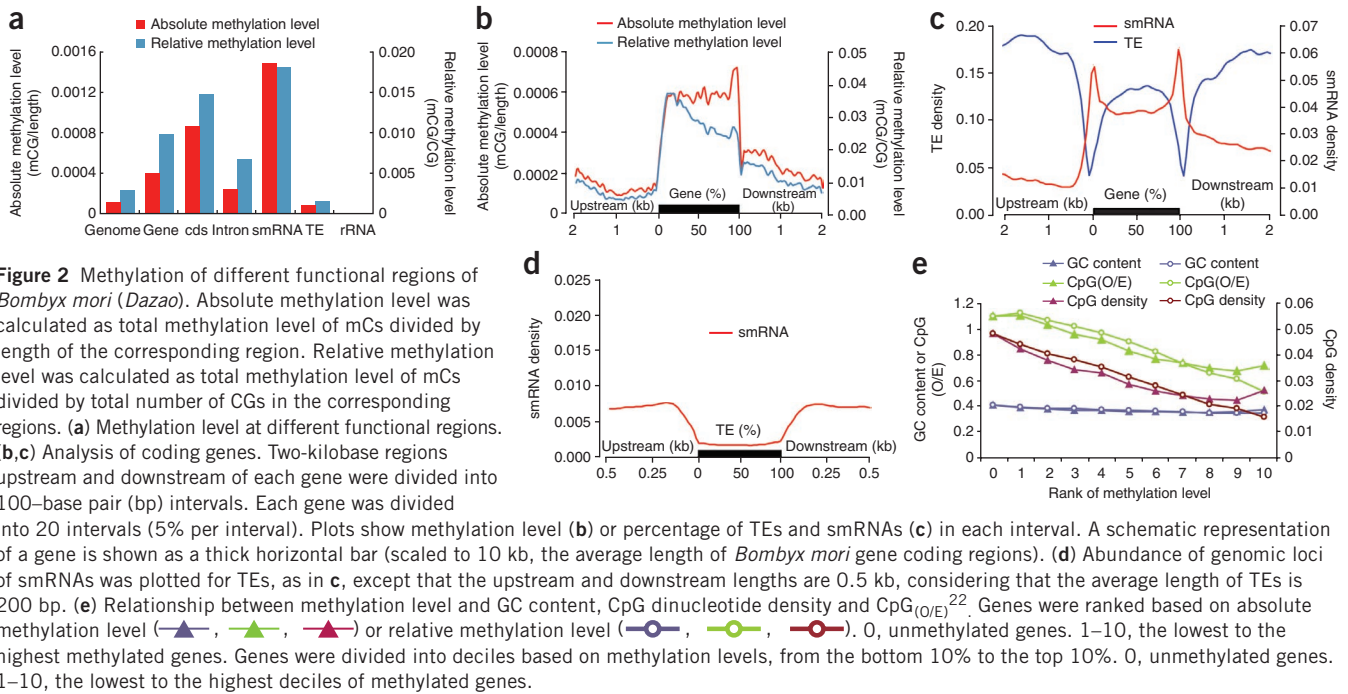
To remove as many of the remaining false positives as possible, we decided to adopt a biological replicate strategy and thus conducted MethylC-Seq on silk gland DNA from a second individual from the same *Dazao* strain. The sequence yield for final analysis is 9.9 Gb, covering 92% of all cytosines in the genome with an average depth of 9.0 × per strand (**Supplementary Table 1**). After the same process of mC identification as used for the first individual, we observed 983,395 mCs, 58.3% Cs of which were at non-CG sites. Comparison of the mCs identified independently in the two individuals revealed a high concordance for mCG sites but overall discordance for mCs at non-CG sites (**Supplementary Fig. 2**). This again indicates that in the silkworm, non-CG mCs are all, or nearly all, false positives, whereas mCGs are frequently genuine.

Although different individuals probably have variable levels of methylation owing to subtle physiological differences, overlap of mCs in two individuals gives a very conservative estimation of real mCs in the *Dazao* silkworm genome. More specifically, 11.3% (65 of 574) of the real mCGs validated by BS-PCR for the first individual were excluded in the final mC map, whereas 99.5% (190 of 191) of false-positive non-CG mCs were excluded (**Supplementary Table 2**).

By combining these two individuals' mCs data, we were able to obtain a high-quality, high-resolution silkworm methylome, with an average read depth of 15 × per strand. In this final DNA methylation map, there are 173,505 mCs, 99.2% of which are at CG sites (**Fig. 1a**), and non-CG mCs, which are still likely to be false positives as suggested by BS-PCR validation (**Supplementary Table 2**), occupy only 0.8% (**Fig. 1a**). BS-PCR validation results indicated that 85.2% (489 of 574) of the total real mCGs in the tested regions were detected by the final map. The conservatively retained mCGs account for 0.11% of all genomic cytosines, which is consistent with previous high-performance liquid chromatography results[7].

We define the methylation level of a specific cytosine as the proportion of reads covering each mC to the total reads covering the site. The majority of mCs have moderate levels of methylation (**Fig. 1b**). CG methylation levels fluctuate drastically across the genome (**Fig. 1c** and **Supplementary Fig. 3**), indicating a mosaic methylation pattern[14], where relatively dense methylated domains are interspersed with regions that are not methylated. This pattern is most frequent in invertebrate animals. Detailed information on strand-specific identification of mCs throughout the whole genome is available at our ftp site (ftp://ftp.genomics.org.cn/silkworm_methylation).

To understand the functional significance of this rather low level of DNA methylation in silkworms, we analyzed the methylation profiles of genes (coding sequences + introns), genomic loci of small RNAs, transposable elements (TEs) and ribosomal DNAs (rDNAs). Both absolute methylation levels (total methylation level of mCs divided by sequence length) and relative methylation levels (total methylation level of mCs divided by total number of CG sites) were used as predictor variables. Notably, methylation within genes, especially coding sequences, is higher than the genome average (**Fig. 2a**). We further calculated methylation levels in the context of gene regions and their 2-kilobase (kb) upstream and downstream regions (**Fig. 2b**). Consistently, both absolute and relative methylation levels are obviously higher within genes. Boundaries between gene bodies and flanking DNA show a sharp drop in methylation (**Fig. 2b**), with 3′ downstream regions showing a little more methylation than 5′ upstream regions. We excluded the contribution of TEs to the enrichment of gene body methylation, as there is a similar

Figure 2 Methylation of different functional regions of *Bombyx mori* (*Dazao*). Absolute methylation level was calculated as total methylation level of mCs divided by length of the corresponding region. Relative methylation level was calculated as total methylation level of mCs divided by total number of CGs in the corresponding regions. (**a**) Methylation level at different functional regions. (**b**,**c**) Analysis of coding genes. Two-kilobase regions upstream and downstream of each gene were divided into 100–base pair (bp) intervals. Each gene was divided into 20 intervals (5% per interval). Plots show methylation level (**b**) or percentage of TEs and smRNAs (**c**) in each interval. A schematic representation of a gene is shown as a thick horizontal bar (scaled to 10 kb, the average length of *Bombyx mori* gene coding regions). (**d**) Abundance of genomic loci of smRNAs was plotted for TEs, as in **c**, except that the upstream and downstream lengths are 0.5 kb, considering that the average length of TEs is 200 bp. (**e**) Relationship between methylation level and GC content, CpG dinucleotide density and CpG$_{(O/E)}$[22]. Genes were ranked based on absolute methylation level ($\triangle$, $\triangle$, $\triangle$) or relative methylation level ($\circ$, $\circ$, $\circ$). 0, unmethylated genes. 1–10, the lowest to the highest methylated genes. Genes were divided into deciles based on methylation levels, from the bottom 10% to the top 10%. 0, unmethylated genes. 1–10, the lowest to the highest deciles of methylated genes.

abundance of TEs within and outside gene regions, and methylation is more prominent in coding sequences than it is in introns (**Fig. 2a,c**). In other insects, such as the aphid and the honeybee, body methylation has also been observed in some genes[5,6,15], and therefore this pattern may be a common feature in insects.

Methylation at genomic sequences that are complementary to small RNAs (smRNAs) is also higher than the genome average for the silkworm (**Fig. 2a**). Notably, these genomic loci matching smRNAs tend to be found in gene bodies but not in TEs (**Fig. 2c,d**). Our analysis showed a significant excess of methylated genomic loci matching smRNA within genes (86.9% of all methylated smRNAs within genes) compared with the genomic background (57.3% of all CG-containing smRNAs within genes) ($P < 0.001$, χ^2 test). In contrast, methylated genomic loci matching smRNA were significantly depleted within TEs (0.5% of all methylated smRNAs in TEs versus 2.9% of all CG-containing smRNAs in TEs, $P < 0.01$, χ^2 test). This pattern contrasts with observations in plants, where highly methylated genomic loci matching smRNAs were barely found in gene bodies but are prevalent in TEs and other repeats (ref. 16 and our unpublished data on rice). In plants, smRNA-directed methylation that targets homologous DNA plays an important role in TE silencing[17], which explains why smRNAs in TEs are highly methylated. smRNAs were also observed to target methylated genes in *Arabidopsis*[18], although this was relatively rare. In silkworms, the prevalence of genomic loci of smRNA in gene bodies and their dense CG methylation imply that smRNAs could be involved in gene body CG methylation.

Methylation in TEs seems to be low compared with the genome average (**Fig. 2a**). Only about 1.2% (5521 of 431,743) of TEs have at least one mCGs, and of these, the majority have low levels of methylation (**Supplementary Fig. 4**), indicating that TEs are usually unmethylated in the *Bombyx* silk gland. In contrast to a recent study[4] on *Drosophila* early embryos that suggested methylation plays a role in transposon silencing, our genome-wide pattern of TE methylation in the silkworm silk gland does not support a general

role for methylation on TEs. We did not observe any mCs in rDNAs, which have been proposed to act as a switch controlling ribosomal gene transcription in plants and mammals[19], implying that, in insects, as suggested by other case studies[20], the regulation of rDNA transcription via methylation has probably not developed.

We found that CG methylation level is not correlated with GC content but with CpG dinucleotide density and CpG observed/expected (O/E) ratio (**Fig. 2e**). CpG O/E ratio is a widely used parameter to predict DNA methylation level based on C→T transition mechanisms resulting from deamination of mCs over the course of evolution[21,22]. Consistent with previous predictions and observations[22,23], genes with higher methylation level tend to have lower CpG dinucleotide and density CpG O/E ratios (**Fig. 2e**).

To reveal the functional consequences of gene body methylation, we generated expression profiles for the two individuals' silk glands using digital gene expression (DGE) tag profiling technology, which uses Illumina high-throughput sequencing as a readout for a classical SAGE (Serial Analysis of Gene Expression) assay. For the two biological replicates, 7,991,117 and 4,620,989 raw reads were generated, and 4,811,597 (60.2%) and 2,435,608 (52.7%), respectively, uniquely mapped to annotated genes. We detected 7,445 and 6,780 annotated genes by at least one unique read (**Supplementary Table 3**). We were also able to detect expression of *Bmdnmt1* and *Bmdnmt2* genes in the DGE data, which is consistent with the results shown by RT-PCR (**Supplementary Fig. 1a**).

We divided genes into five groups based on expression levels, from the bottom 20% to the top 20%. Notably, we observed that methylation level is positively correlated with expression level in both individuals (**Fig. 3a** and **Supplementary Fig. 5a**). A similar pattern was observed when grouping genes by their methylation levels (**Fig. 3b** and **Supplementary Fig. 5b**). The observed correlations are supported by Spearman correlation analyses (**Fig. 3c** and **Supplementary Fig. 5c**). This result suggests that gene body methylation may be an ancient system, because the same pattern has been reported in plants and chordates[18,23]. However, no correlation between expression level and
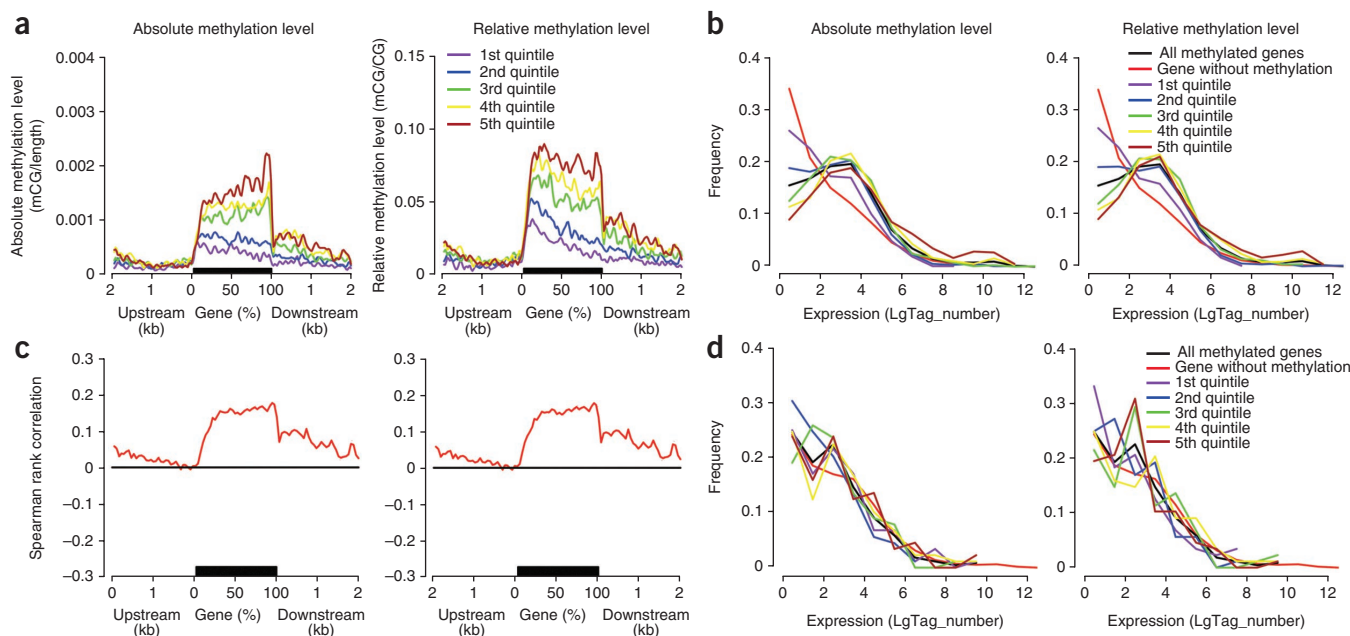
Figure 3 Relationship between DNA methylation and expression levels of genes in *Bombyx mori* (*Dazao*). (**a**) Methylation level within gene bodies divided by expression level. Genes were classified into quintiles based on expression: 1st quintile is lowest and 5th is highest. Two-kilobase regions upstream and downstream of each gene were divided into 100-bp intervals. Each gene was divided into 20 intervals (5% per interval). Plots show the methylation level of each interval. (**b**) Expression of methylated compared with unmethylated genes. Genes were rank-ordered based on gene body methylation level and divided into quintiles. For the methylated genes, 1st quintile is the lowest and 5th is the highest. (**c**) Spearman correlation index between methylation level and gene expression level. Two-kilobase regions upstream and downstream of each gene were divided into 100-bp intervals. Each gene was divided into 20 intervals (5% each interval). Plots show the Spearman correlation index of each interval. (**d**) The same as **b**, except for promoter methylation. Absolute and relative methylation levels were calculated as described for **Figure 2**.

methylation level in the promoter regions was detected (**Fig. 3d** and **Supplementary Fig. 5d**), which suggests that the well-known gene regulatory function of promoter methylation in plants and mammals[17,24,25] may not operate in insects.

We further used the BGI WEGO (Web Gene Ontology Annotation Plotting)[26] to functionally categorize the methylated and unmethylated

genes and observed significant differences (**Fig. 4a**). Methylated genes tend to be enriched in binding activities, including translation regulators. As for biological processes, they are enriched in functions associated with cellular metabolic and biosynthetic processes as well as cellular response to stimulus. In contrast, unmethylated genes are enriched in transcription regulators, such as transcription factors, and
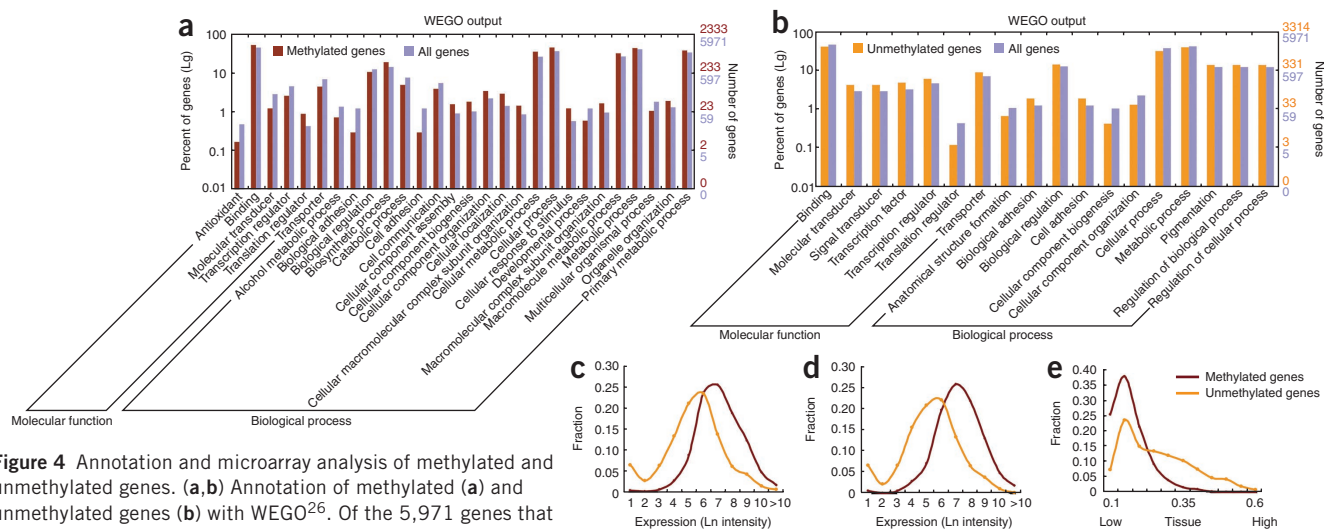

Figure 4 Annotation and microarray analysis of methylated and unmethylated genes. (**a**,**b**) Annotation of methylated (**a**) and unmethylated genes (**b**) with WEGO[26]. Of the 5,971 genes that have GO annotations, 2,333 methylated and 3,314 unmethylated genes showed significant enrichment difference ($P < 0.05$, χ^2 test) compared with total analyzed genes. Annotations are grouped by molecular function or biological process based on the silkworm *Bombyx mori* GO annotation information (ftp://silkdb.org/pub/current/otherdata/Gene_ontology/silkworm_glean_gene.go). Gene numbers and percentages (on log scale) are listed for each category. (**c**,**d**) Expression in the anterior-mid silk gland (**c**) and posterior silk gland (**d**) of methylated and unmethylated genes examined by microarray analysis. (**e**) Tissue expression specificity of methylated and unmethylated genes measured by τ value[27].

transducers and transporters. Unmethylated genes are also enriched in functions associated with regulation and adhesion processes. We confirmed that methylated genes tend to be more highly expressed than unmethylated genes in the silk gland (**Fig. 4b,c**) by analyzing the relationship between gene body methylation and tissue expression specificity using the available microarray data from *B. mori* tissues on day three of the fifth-instar larvae (BmMDB: http://silkworm.swu.edu.cn/microarray/). We suspect that methylation may contribute to maintaining the relatively high expression of genes that are essential for biosynthetic processes in the silk gland. Furthermore, methylated genes showed lower tissue specificity (**Fig. 4d**), which was also observed in *Arabidopsis*[24].

In conclusion, we have generated the first, to our knowledge, single base–resolution methylome for an insect species. We found that MethylC-Seq has a considerable false-positive rate in detecting mCs in species with low methylation level. Thus, effective removal of these false positives is very important before any functional analysis. In this study, we used non-CG mCs as the background control in conjunction with a biological replicate strategy. Together, these controls identified methylated CG sites that could be validated by low-throughput assays. This high-quality single-base DNA methylome map supports the functional significance of the rather low methylation in the silkworm and indicates that the well-established functions of methylation on TEs, rDNAs and promoters in plants and mammals may not be well developed in insects. This DNA methylome map will be useful for further studies on epigenetic gene regulation in silkworm and other insects. Moreover, the active epigenetic system existing in the silkworm lays a foundation for exploring the contributions of epigenetics to silkworm domestication.

METHODS
Methods and any associated references are available in the online version of the paper at http://www.nature.com/naturebiotechnology/.

Accession codes. Sequence data is available under the GEO accession GSE18315 and the SRA accession SRP001159.

Note: Supplementary information is available on the Nature Biotechnology website.

AUTHOR CONTRIBUTIONS
J.W., W.W., J.Z. and Q.X. designed the study. H.X., W.W. and X.L. wrote the manuscript. X.L., G.Z., Q.C., Y.L. and R.L. developed the method for mapping and processing BS reads. D.L. and D.C., performed microarray analysis. F.D. and M.L. provided the domestic silkworm samples and detailed background information on silkworm domestication and breeding. H.X. and X.L. analyzed the 454 data. H.X.

did RT-PCR. Y.D. performed the methyltransferase assay. H.X., Y.L., Q.G. and J.J. extracted DNAs and RNAs. J.Z., H.Z., J.Y., J.S., X.Z., K.M., L.Z., Y.H., S.G. and Y.Z. constructed the BS-seq libraries and conducted the BS validation. G.G., X.Z., L.M., M.Y. and K.K. performed the Solexa sequencing. S.B. contributed to the interpretation of the results. All authors have read and contributed to the manuscript.

1. Lister, R. *et al.* Highly integrated single-base resolution maps of the epigenome in *Arabidopsis*. *Cell* **133**, 523–536 (2008).
2. Lister, R. *et al.* Human DNA methylomes at base resolution show widespread epigenomic differences. *Nature* **462**, 315–322 (2009).
3. Regev, A., Lamb, J.M. & Jablonka, E. The role of DNA methylation in invertebrates: developmental regulation or genome defense? *Mol. Biol. Evol.* **15**, 880–891 (1998).
4. Patel, C.V. & Gopinathan, K.P. Determination of trace amounts of 5-methylcytosine in DNA by reverse-phase high-performance liquid chromatography. *Anal. Biochem.* **164**, 164–169 (1987).
5. Field, L.M. Methylation and expression of amplified esterase genes in the aphid *Myzus persicae* (Sulzer). *Biochem. J.* **349**, 863–868 (2000).
6. Wang, Y. *et al.* Functional CpG methylation system in a social insect. *Science* **314**, 645–647 (2006).
7. Phalke, S. *et al.* Retrotransposon silencing and telomere integrity in somatic cells of *Drosophila* depends on the cytosine-5 methyltransferase DNMT2. *Nat. Genet.* **41**, 696–702 (2009).
8. Xiang, Z. *Genetics and Breeding of the Silkworm* (Chinese Agriculture Press, Beijing, P.R. China, 1995).
9. Kalisz, S. & Purugganan, M.D. Epialleles via DNA methylation: consequences for plant evolution. *Trends Ecol. Evol.* **19**, 309–314 (2004).
10. Farcas, R. *et al.* Differences in DNA methylation patterns and expression of the CCRK gene in human and nonhuman primate cortices. *Mol. Biol. Evol.* **26**, 1379–1389 (2009).
11. Schaefer, M. & Lyko, F. DNA methylation with a sting: an active DNA methylation system in the honeybee. *Bioessays* **29**, 208–211 (2007).
12. Uno, T. *et al.* Expression, purification and characterization of methyl DNA binding protein from *Bombyx mori*. *J. Insect Sci.* **5**, 8 (2005).
13. Xia, Q. *et al.* A draft sequence for the genome of the domesticated silkworm (*Bombyx mori*). *Science* **306**, 1937–1940 (2004).
14. Suzuki, M.M. & Bird, A. DNA methylation landscapes: provocative insights from epigenomics. *Nat. Rev. Genet.* **9**, 465–476 (2008).
15. Mandrioli, M. & Borsatti, F. DNA methylation of fly genes and transposons. *Cell. Mol. Life Sci.* **63**, 1933–1936 (2006).
16. Cokus, S.J. *et al.* Shotgun bisulphite sequencing of the *Arabidopsis* genome reveals DNA methylation patterning. *Nature* **452**, 215–219 (2008).
17. Zhang, X. The epigenetic landscape of plants. *Science* **320**, 489–492 (2008).
18. Zilberman, D., Gehring, M., Tran, R.K., Ballinger, T. & Henikoff, S. Genome-wide analysis of *Arabidopsis thaliana* DNA methylation uncovers an interdependence between methylation and transcription. *Nat. Genet.* **39**, 61–69 (2007).
19. Lawrence, R.J. & Pikaard, C.S. Chromatin turn ons and turn offs of ribosomal RNA genes. *Cell Cycle* **3**, 880–883 (2004).
20. Mandrioli, M. & Borsatti, F. Analysis of heterochromatic epigenetic markers in the holocentric chromosomes of the aphid *Acyrthosiphon pisum*. *Chromosome Res.* **15**, 1015–1022 (2007).
21. Elango, N., Kim, S.H., Vigoda, E. & Yi, S.V. Mutations of different molecular origins exhibit contrasting patterns of regional substitution rate variation. *PLOS Comput. Biol.* **4**, e1000015 (2008).
22. Elango, N., Hunt, B.G., Goodisman, M.A. & Yi, S.V. DNA methylation is widespread and associated with differential gene expression in castes of the honeybee, *Apis mellifera*. *Proc. Natl. Acad. Sci. USA* **106**, 11206–11211 (2009).
23. Suzuki, M.M., Kerr, A.R., De Sousa, D. & Bird, A. CpG methylation is targeted to transcription units in an invertebrate genome. *Genome Res.* **17**, 625–631 (2007).
24. Zhang, X. *et al.* Genome-wide high-resolution mapping and functional analysis of DNA methylation in *Arabidopsis*. *Cell* **126**, 1189–1201 (2006).
25. Weber, M. *et al.* Distribution, silencing potential and evolutionary impact of promoter DNA methylation in the human genome. *Nat. Genet.* **39**, 457–466 (2007).
26. Ye, J. *et al.* WEGO: a web tool for plotting GO annotations. *Nucleic Acids Res.* **34**, W293–297 (2006).
27. Liao, B.Y. & Zhang, J. Low rates of expression profile divergence in highly expressed genes and tissue-specific genes during mammalian evolution. *Mol. Biol. Evol.* **23**, 1119–1128 (2006).

ONLINE METHODS

Expression of *Dnmt1* and *Dnmt2* genes evaluated by RT-PCR. Total RNAs were extracted from different developmental stages (8-h-old, 3-day-old, 7-day-old and 10-day-old eggs; 1st- to 4th-instar larvae; young and old pupae; adults of the silkworms), as well as from different tissues including heads, cuticle, silk glands, guts, ovaries, and testis from the 5th-instar larvae of silkworms, using Trizol (Invitrogen). Total RNA was digested with DNase I (Takara) to remove remaining DNA. Complementary DNA (cDNA) was synthesized using the RevertAid First Strand cDNA Synthesis Kits (Fermentas). Expression of *Dnmt1* and *Dnmt2* genes was evaluated by RT-PCR using primers listed in **Supplementary Table 4** with 30 cycles (30 min at 94 °C, 30 min at 54 °C and 30 min at 72 °C) for cDNA templates derived from materials of different developmental stages, and 34 cycles (30 min at 94 °C, 30 min at 54 °C and 30 min at 72 °C) for cDNA templates derived from different tissues, respectively.

Nuclear protein extraction and assay of DNA methyltransferase activity. About 150 mg of silkworm eggs or one silk gland from one silkworm individual were ground into powder in liquid nitrogen and homogenized in 150 μl tissue homogenization buffer (10 mmol HEPES-KOH (pH 7.6), 25 mmol KCl, 0.15 mmol spermine, 0.5 mmol spermidine, 2 mol sucrose, 10% (v/v) glycerol, 1 mmol EDTA). Homogenate was held on ice for 30 min and then centrifuged at 3000*g* for 15 min at 4 °C to obtain the protein precipitate. The protein precipitate was resuspended in 650 μl resuspension buffer (5 mmol HEPES-KOH (pH 7.9), 0.5 mmol phenylmethylsulfonyl fluoride, 26% (v/v) glycerol, 0.5 mmol dithiothreitol, 1.5 mmol MgCl$_2$) and then centrifuged at 14,000*g* for 45 min at 4 °C to obtain soluble proteins. Protein concentration was determined by the Bio-Rad Protein Assay kit (Bio-Rad). Three independent replicate protein samples were prepared for each material.

About 15 μg nuclear protein extracts from either eggs or silk gland and equal amount of the negative control (bovine serum albumin) were respectively analyzed for DNA methyltransferase activity using the EpiQuik DNA Methyltransferase Activity/Inhibition Assay Kit (Epigentek) following the manufacturer's instructions. Pure mouse DNMT1 in the kit was used as the positive control. Methyltransferases activity is indicated by the average absorbance at 450 nm (OD$_{450}$).

Sample preparation for MethylC-Seq and digital gene expression analyses. Each silk gland of 5th-instar larvae of two individuals (called biological replicate 1 and 2, respectively) of the silkworm (*B. mori*) strain *Dazao* was ground into powder in liquid nitrogen. Half of the powder from each silk gland was used to extract total DNAs using DNeasy Blood and Tissue Kit (Qiagen), and the other half was used to extract total RNAs using RNeasy Mini Kit (Qiagen).

MethylC-Seq library construction and sequencing. DNA was fragmented by sonication with a Sonicator (Sonics & Materials) to a mean size of approximately 250 bp, followed by blunt ending, 3′-end addition of dA, and adapter ligation, in which Illumina methylated adapters were used according to the manufacturer's instructions (Illumina). The bisulfite conversion of silkworm DNA was carried out using a modified NH$_4$SO$_4$-based protocol[28] and amplified by 12 cycles of PCR. Ultra-high-throughput pair-end sequencing was carried out using the Illumina Genetic Analyzer (GA2) according to manufacturer instructions. Raw GA sequencing data were processed by Illumina base-calling pipeline (SolexaPipeline-1.0).

Digital gene expression (DGE) tag libraries and sequencing. DGE tag libraries were constructed using the silk gland RNAs and the DGE-Tag Profiling NlaIII Sample Prep Kit (Illumina). Libraries were sequenced using the Illumina Genetic Analyzer (GA2) according to the manufacturer's instruction. Raw GA sequencing data were processed by Illumina base-calling pipeline (SolexaPipeline-1.0).

Mapping and initial processing of MethylC-Seq reads. Short reads with 44-nucleotide (nt) reads or 75-nt reads from each end generated by Illumina sequencing were aligned to the *Dazao* reference genome. *B. mori* (*Dazao*) reference genome sequences were downloaded from the SilkDB (ftp://silkdb.org/pub/current/Genome/silkworm_genome_v2.0.fa.tar.gz).

Because DNA methylation has strand specificity, the plus strand and the minus strand of the *Dazao* genome should be separated and formed alignment target sequences. That is, each cytosine in genome sequences was converted to thymine, termed T-genome, which represents the plus strand. Meanwhile, each guanine in genome sequences was converted to adenosine, termed A-genome, which represents the minus strand. In addition, the original reads were also computationally transformed to the alignment forms with the following steps: (i) observed cytosines on the forward read of each read pair were *in silico* replaced by thymines; (ii) observed guanines on the reverse read of each read pair were *in silico* replaced by adenosines.

We used the software named SOAPaligner[29], allowing up to two mismatches for mapping both 44-nt pair-end reads (for the biological replicate 1) and up to four mismatches for 75-nt pair-end reads (for the biological replicate 2) to map the computationally transformed reads to the alignment target sequences. Multiple reads mapped to the same start position were regarded as clonal duplication, which might be generated during PCR process, and only one of them was kept. For mC detection, we transformed each aligned read and the two strands of the *Dazao* genome back to their original forms to build an alignment between the original forms. Cytosines in the MethylC-seq reads that are also matched to the corresponding cytosines in the plus (Watson) strand, or otherwise guanines in the MethylC-seq reads that are also matched to the corresponding guanines in the minus (Crick) strand will be regarded as potential mCs. Q score, which is used in base-calling pipeline (SolexaPipeline-1.0) (Illumina) to detect sequences from the raw fluorescent images, is calculated as:

$$Q = 10 \log_{10} \left[p(X) / (1 - p(X)) \right]$$

where $p(X)$ is the probability that a read is correctly called. We then carried out a filtering process to filter out all potential mCs with Q scores smaller than 20, guaranteeing that a base is correctly called at more than 99% probability, highly conservative for calling reliable bases.

Bisulfite-PCR validation for target regions using either Sanger sequencing or 454 sequencing. One microgram of genomic DNA from the silk gland of biological replicate 1 was bisulfite-converted following the same protocol for constructing the MethylC-Seq library. Primers were designed to amplify a batch of target regions of the bisulfite-converted DNA for validation of the MethylC-Seq results. Initially, we validated five target regions containing 26 mCGs detected by MethylC-Seq and three target regions containing one mCHG and 98 clustered mCHHs detected by MethylC-Seq by Sanger sequencing multiple independent TA clones for each PCR product. Then we further used 454 sequencing technique (454 Life Sciences) to confirm 107 PCR products in total (692 mCGs, 29 mCHGs and 63 mCHHs). We pooled PCR products of these fragments, and the 454 sequencing library was constructed according to the manufacturer's instruction (454 Life Sciences). Eventually we obtained sequencing data on 6,698,205 bp. BLAST searches (e-value <1e$^{10-3}$) against the original target sequence database were performed to map the raw reads. Matched sequences with length ≥30 bp were used for further calculation of methylation level at each single cytosine site. All the primers were listed in **Supplementary Table 4**.

mC identification and removal of background noises. All of the tested mCHGs and mCHHs initially detected by MethylC-Seq are proved to be false positive by bisulfite-PCR validation, indicating that non-CG mCs are either very rare or all false positive (**Supplementary Table 2**). Therefore, we first checked the mCs detected by initial MethylC-Seq of each biological replicate. If the next base of mC at a non-CG site in the read is actually G, it should be a false-positive non-CG methylation but a possible CG methylation due to polymorphism in different individuals. However, to be conservative we uniformly exclude these potential single-nucleotide polymorphism-caused mCs. We then used the methylation rate at non-CG sites of the whole genome as the background noise control, which provides a measure for the false-positive rate (sum of the nonconversion rate and thymidine-to-cytosine sequencing errors):

$$\text{False-positive rate} = (n_{\text{mCHG}} + n_{\text{mCHH}}) / n_{\text{depth}} \times 100\%$$

Where n_{mCHG} and n_{mCHH} refer to the total number of sequenced Cs in the CHG and CHH contexts in the reference genome, respectively. n_{depth} refers to the total sequenced depth at cytosine positions in CHG and CHH contexts in the reference genome. Using this value as a measure of the false mC discovery rate, following the correction algorithm of Lister *et al.*[2], we set a significance threshold (99% confidence) to identify the presence of an mC determined at each base position based on the binomial probability distribution, read depth and the calculated false-positive rate. mCs that are below the minimum threshold at a site were rejected.

Despite these filtrations, the non-CG methylation noises still occupied a considerable proportion, because a proportion of non-CG mCs appeared in high methylation levels in the original MethylC-Seq data. Because our bisulfite-PCR validation showed that even high-methylation-level mCs are false positive, to effectively remove these noises we decided to use a strategy of biological replicates and thus compared the mCs independently identified in both replicates and found that a large proportion of the mCGs are consistently detected in both replicates, whereas mCs in non-CG contexts are nearly replicate-specific (**Supplementary Fig. 1**), further confirming that non-CG mCs are either all false positive or very rare, whereas mCGs are largely real in the silkworm. In this way we effectively removed background noises and finally generated a methylome map with high reliability and high resolution (on average each cytosine in the genome is covered by 15 reads).

Mapping and processing DGE tags. Sequence information of the *Bombyx mori* genes was downloaded from the SilkDB (ftp://silkdb.org/pub/current/Gene/Glean_genes/silkworm_glean_cds.fa.tar.gz). Gene annotation information was downloaded from the SilkDB (ftp://silkdb.org/pub/current/Gff/silkworm_glean.gff.tar.gz). Because annotated genes were mainly predicted using prediction software, only open reading frame positions were available. We created putative full-length cDNA sequences for each gene by adding 1-kb downstream sequences of open reading frame to coding sequences. Then all possible CATG + 17 nt tag sequences were created from putative full-length cDNAs and used as a reference tag database. Unique tag sequences and their numbers were extracted from our raw DGE tags, and these tags were aligned against the reference tag database using SOAP[30]. Only perfect matches were kept for further analysis, and no mismatches were allowed. Expression level of one gene was represented by the total number of tags that uniquely aligned to this gene.

Analyses on abundance of TEs and genomic loci of smRNAs. Annotation of known TEs was downloaded from the SilkDB (ftp://silkdb.org/pub/current/Gff/Public_ReAS_TEs/silkworm_Publicknow_TE.gff.tar.gz). The smRNA sequences were downloaded from the GenBank (http://www.ncbi.nlm.nih.gov/geo/query/acc.cgi?acc=GSE17965). Sequences of smRNAs were mapped to the reference genome using SOAP[30] without mismatch, and uniquely mapped smRNAs were used for further analysis. TE and smRNA densities were defined as the ratios of number of bases that belong to TEs or smRNAs divided by the total length of the calculated regions.

Gene ontology (GO) annotation. GO annotations of silkworm genes were downloaded from the SilkDB (ftp://silkdb.org/pub/current/otherdata/Gene_ontology/silkworm_glean_gene.go). GO comparative analyses between interested gene groups were performed using BGI WEGO (http://wego.genomics.org.cn/cgi-bin/wego/index.pl)[26].

Microarray analysis. The microarray data of the analyzed genes were obtained from the *B. mori* microarray database (BmMDB: http://silkworm.swu.edu.cn/microarray/). Tissue specificity index τ[27] is used to measure the tissue specificity of a silkworm gene, which is defined as:

$$\tau_H = \frac{\sum_{j=1}^{n_H}\left(1 - \left[\frac{\log_2 S_H(i,j)}{\log_2 S_H(i,\max)}\right]\right)}{n_H - 1}$$

where n_H is the number of female silkworm tissues examined and $S_H(i,\max)$ is the highest expression signal of gene i across the n_H tissues. To minimize the influence of noise from low intensity, we arbitrarily let $S_H(i,j)$ be 100 if it is lower than 100. The τ value ranges from 0 to 1, with higher values indicating higher tissue specificity. Genes with the highest expression signal of a certain tissue were considered as expressionally upregulated in this tissue.

28. Hayatsu, H., Tsuji, K. & Negishi, K. Does urea promote the bisulfite-mediated deamination of cytosine in DNA? Investigation aiming at speeding-up the procedure for DNA methylation analysis. *Nucleic Acids Symp. Ser.* **50**, 69–70 (2006).
29. Li, R. *et al*. SOAP2: an improved ultrafast tool for short read alignment. *Bioinformatics* **25**, 1966–1967 (2009).
30. Li, R., Li, Y., Kristiansen, K. & Wang, J. SOAP: short oligonucleotide alignment program. *Bioinformatics* **24**, 713–714 (2008).

Corrigendum: Safety signal dampens reception for mipomersen antisense

Jim Kling
Nat. Biotechnol. **28**, 295–297 (2010); published online 8 April 2010; corrected after print 9 July 2010

In the version of this article initially published, some of the oligos in Table 1 are described as phosphorothioate modified. In fact, all antisense oligonucleotides are phosphorothioate-modified oligos. In addition, Lucanix, which is not an antisense oligo, has been removed from the table. The error has been corrected in the HTML and PDF versions of the article.

Corrigendum: *Ab initio* reconstruction of cell type–specific transcriptomes in mouse reveals the conserved multi-exonic structure of lincRNAs

Mitchell Guttman, Manuel Garber, Joshua Z Levin, Julie Donaghey, James Robinson, Xian Adiconis, Lin Fan, Magdalena J Koziol, Andreas Gnirke, Chad Nusbaum, John L Rinn, Eric S Lander & Aviv Regev
Nat. Biotechnol. **28**, 503–510 (2010); published online 02 May 2010; corrected after print 9 July 2010

In the version of this article initially published, the fourth sentence in the Online Methods section "RNA extraction and library preparation," that read in part "procedure that combines a random priming step with a shearing step[8,9,28] and results in fragments of ~700 bp in size," should have read, "procedure that combines fragmentation of mRNA to a peak size of ~750 nucleotides by heating[6] followed by random-primed reverse transcription[8]." The error has been corrected in the HTML and PDF versions of the article.

Erratum: US biodefense contracts continue to lure biotechs

Catherine Shaffer
Nat. Biotechnol. **28**, 187–188 (2010); published online 8 March 2010; corrected after print DD Month 9 July 2010

In the version of this article initially published, in Table 1, the Emergent BioSolutions' anthrax countermeasures in development listed AV-7909 as being in phase 2 under a $447.6 million BARDA contract; AV-7909 is in phase 1 and the BARDA contract is for $29.7 million. AIGIV is in phase 1/3, not phase 1/2. Finally, a third product was omitted; anthrax monoclonal is in preclinical testing under a $24 million BARDA contract. The $447.6 million BARDA contract was for procurement and product enhancements on BioThrax. Also, on p.188, column 2, line 7, the vaccine requires five injections, not six as originally stated. The error has been corrected in the HTML and PDF versions of the article.

Erratum: Single base–resolution methylome of the silkworm reveals a sparse epigenomic map

Hui Xiang, Jingde Zhu, Quan Chen, Fangyin Dai, Xin Li, Muwang Li, Hongyu Zhang, Guojie Zhang, Dong Li, Yang Dong, Li Zhao, Ying Lin, Daojun Cheng, Jian Yu, Jinfeng Sun, Xiaoyu Zhou, Kelong Ma, Yinghua He, Yangxing Zhao, Shicheng Guo, Mingzhi Ye, Guangwu Guo, Yingrui Li, Ruiqiang Li, Xiuqing Zhang, Lijia Ma, Karsten Kristiansen, Qiuhong Guo, Jianhao Jiang, Stephan Beck, Qingyou Xia, Wen Wang & Jun Wang
Nat. Biotechnol. **28**, 516–520 (2010); published online 02 May 2010; corrected after print 9 July 2010

In the version of this article initially published, references 4 and 7 were inadvertently interchanged. The error has been corrected in the HTML and PDF versions of the article.

Erratum: Up for grabs

Michael Eisenstein
Nat. Biotechnol. **28**, 544–546 (2010); published online 7 June 2010; corrected after print 9 July 2010

In the version of the article originally published, it was stated that the Cohen-Boyer patents generated hundreds of billions of dollars in licensing revenue. It should have read hundreds of millions of dollars. The error has been corrected in the HMTL and PDF versions of the article.